On the Conversion of $\text{He}(2^3S)$ to $\text{He}_2(a^3\Sigma_u^+)$

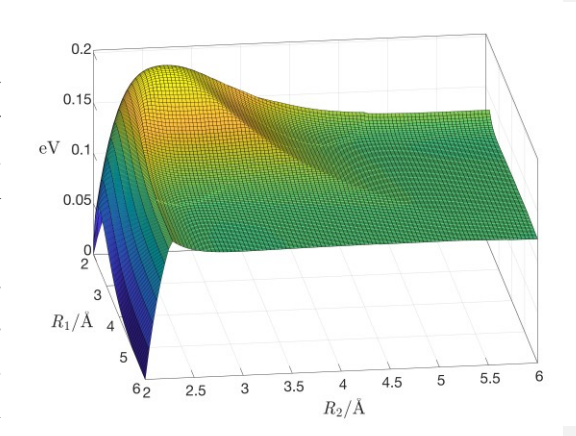
P. Nijjar, A. I. Krylov, O. V. Prezhdo, A. F. Vilesov,* and C. Wittig*

Department of Chemistry

University of Southern California

Los Angeles, CA 90089

ABSTRACT: The report of an anomalously intense He₄⁺ peak in mass spectra of large helium droplets created a stir three decades ago that continues to this day. When the electron kinetic energy exceeds 41 eV, an additional pathway to He₄⁺ opens that yields He₄⁺ predominantly in an electronically excited metastable state. A pair of He* (2³S) atoms has been implicated based on the isolated



He* energy of 19.82 eV and the 41-eV threshold. The creation of He_4^+ has been conjected to proceed via a pair of $\text{He}_2^*(a^3\Sigma_u^+)$ precursors, whose formation mechanism remains poorly understood. High level ab initio theory combined with classical molecular dynamics has been applied to systems comprising small numbers of He atoms. Conversion of He* to He₂* in such systems was found to be rapid and efficient. We conclude that He_2^* is a likely participant in the production of He_4^+ on surfaces of large helium droplets.

^{*} Corresponding authors: vilesov@usc.edu; wittig@usc.edu.

Superfluid helium droplets serve as a unique platform upon which a broad range of interesting and at times intriguing phenomena have been discovered and examined.¹⁻⁶ Indeed, many of the experimental results that have accrued throughout the past several decades have proven seminal. They have often been rationalized using qualitative models, with the understanding that detailed mechanistic pictures are likely more complicated, or perhaps even deviate significantly from the original models.

The mechanism of the anomalously effective production of He₄⁺ ions upon electron bombardment of large helium droplets has remained elusive for 30 years. To understand this anomaly, we apply a computational approach that combines high level ab initio theory with molecular dynamics (MD) simulations. It enables us to analyze in detail small model systems consisting of a few He atoms, thereby obtaining insights that are germane to larger systems, notably helium droplets.

The experimental studies that motivated the present work used electron impact excitation to create the lowest energy triplet, He* (2^3S), within helium droplets.⁷ Hereafter, He* and He₂* ($a^3\Sigma_u^+$) within and on bulk helium and helium droplets shall be referred to simply as He* and He₂*. They are often referred to as metastable because of their long radiative lifetimes and the fact that they do not autoionize or dissociate. Of course, they can interact rapidly with atoms, molecules, etc.

The saga began with a fascinating result obtained in a mass spectrometric study of large superfluid helium droplets by Buchenau et al.⁸⁻⁹ Plots of He_n^+ signal intensity versus n displayed an anomaly when the electron kinetic energy (eKE) exceeded roughly 40 eV. Rather than decaying monotonically with n, as in small droplets, ^{8, 10-15} the He_4^+ signal was an order of magnitude more intense than expected. The authors concluded that pairs of He^* atoms created within large droplets are the progenitors of the enhanced He_4^+ production, as the energy of isolated He^* is 19.82 eV. They proposed that an incident electron creates He^* , and then goes on to create a second He^* within the same droplet, and that He^* might convert to He_2^* on droplet surfaces. Schöbel et al. established the threshold by showing that the slope of He_4^+ yield versus eKE increases sharply at 41 eV.¹³

Earlier, Keto et al. $^{16-18}$ and Hill et al. 19 had shown that He₂* and He* are produced when superfluid helium is bombarded with 160 keV electrons. The He₂* was removed by He₂* + He₂* \rightarrow products (though the products were not identified). Keto et al. showed that He* was removed by

bulk helium with a temperature independent 15 μ s exponential decay. ¹⁶⁻¹⁸ They also assigned two low resolution spectral features to high vibrational levels of $a^3\Sigma_u^+$ (Figure 1), and suggested that such high- ν levels might be due to He* combining with He. Each 160 keV electron resulted

in ≈ 500 He* atoms, and about the same number of He₂* molecules, via myriad cascades, which made interpretation challenging. Brooks et al. confirmed the presence of high vibrational levels ($\nu = 10$ -12) following bombardment of dense cryogenic gas with 6.5 MeV protons.²⁰ Northby and coworkers found that, in addition to N=1, highly rotationally excited He₂* ($11 \le N \le 29$) survives on droplet surfaces for at least 4 ms.²¹⁻²⁴ They concluded that the precursor is He(2^3P), whose gas phase energy is 20.96 eV. They showed that He* was not responsible for the He₂* they obser-

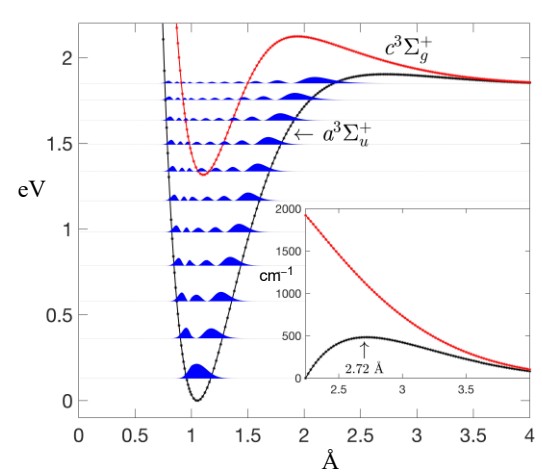


Figure 1. The $a^3\Sigma_u^+$ and $c^3\Sigma_g^+$ potential energy curves correlate to He* + He. The vertical scale for the $a^3\Sigma_u^+$ barrier region is expanded in the insert.

ved, and noted that $\text{He}(2^3P)$ correlates without a barrier to the $b^3\Pi_g$ state (which radiates to $a^3\Sigma_u^+$) as opposed to the barrier on $a^3\Sigma_u^+$ (Figure 1). Their spectra did not include a region where transitions originate from He_2^* high vibrational levels.

Experiments by von Issendorff et al. ¹⁵ and an electronic structure study by Knowles and Murrell ²⁵⁻²⁶ concluded that metastable $He_4^+(^4A_2)$ is responsible for the anomaly. Its energy relative to 4 He atoms is 38.93 eV, which is consistent with the energy of two He* atoms (39.64 eV) and the 41-eV threshold. Fine et al. found that the time required for metastables on surfaces of large droplets to undergo associative ionization to He_4^+ was roughly 10 μ s under their experimental conditions. ²⁷ They argued that excited species (He*, He₂*) travel to droplet surfaces with minimal encounter with one another along the way, and that without theory the potentially reactive combinations $He^* + He^*$, $He^* + He_2^*$, and $He_2^* + He_2^*$ cannot be distinguished.

• //do we need a bullet point here? It makes an ident to the following paragraph// One thing is certain: He* created at t = 0 exists in a transient local helium environment that is rife with complexity, meaning that questions abound. For example, does He* create a bubble, or, alternatively, does it convert to He₂* which then creates a bubble?²⁸⁻³⁰ The conversion of He* to He₂* is central, as it dictates which species arrive at surfaces of large droplets. In fact, it is relevant to all studies that involve electron impact creation of metastables in superfluid helium.

Figure 1 illustrates the essence of the puzzle. The He₂* potential has a bond strength of 14,833 cm⁻¹ relative to He* + He, $^{31-32}$ and an entrance barrier that can be understood qualitatively as repulsion between Rydberg electron density and a He atom, countered by attraction between the partially shielded He⁺ core and the He atom. We find that this barrier peaks at 2.72 Å, with energy of 516 cm⁻¹ relative to He* + He, in accord with previous studies. 28,33 The potential is quite flat in this region, down from its peak by only 0.5 cm⁻¹ at 2.70 and 2.74 Å. This barrier seems insurmountable at T = 0.4 K in helium droplets. 34 Yet, we shall explain how He₂* can be formed efficiently.

We interrogated this issue by using the equation-of-motion coupled-cluster method with single and double substitutions for excitation energies (EOM-EE-CCSD),³⁵⁻³⁶ and for diffuse wave functions of Rydberg states, we used the d-aug-cc-pVDZ basis (see SI and Computational Details). Natural transition orbitals (NTOs)³⁷⁻⁴⁰ provide insight into correlated excited states. By performing singular value decomposition of one-particle transition density, NTOs provide the most compact description of electronic transitions in terms of pairs of molecular orbitals.

We began with a model in which 3 He atoms are constrained to a straight line (Figure 2a). The first item of interest was the energy landscape of the lowest triplet adiabat (analogous to $a^3\Sigma_u^+$ in Figure 1) and its electronic character, as revealed by NTOs. We then carried out MD simulations using potentials computed "on the fly." Trajectories were launched from initial interatomic distances R_1^0 and R_2^0 with zero kinetic energy// would leave out because non-zero kinetic energy is essential for superfluidity:, consistent with superfluid conditions//. The trajectories were propagated for 484 fs (see SI). Values of R_1^0 and R_2^0 were chosen to be in accord with the superfluid helium radial distribution function (*vide infra*, Figure 5).⁴¹⁻⁴³ We then extended the model to 4

atoms constrained to a straight line and 3-atom nonlinear geometries (Figures 2b and 2c, respectively). A few results are given for 10-atom systems confined to a plane.

Such systems can prove subtle. Creation of the lowest triplet adiabat at t=0 endows it with initial interatomic distances characteristic of superfluid helium. This results in weak attractive and repulsive interactions that launch, and participate in, the ensuing dynamics, which can result in the formation of He₂*. How these dynamical processes play out is not obvious *a priori*, motivating detailed analyses. A complete theoretical description includes non-adiabatic transitions among multiple adiabats, e.g.,

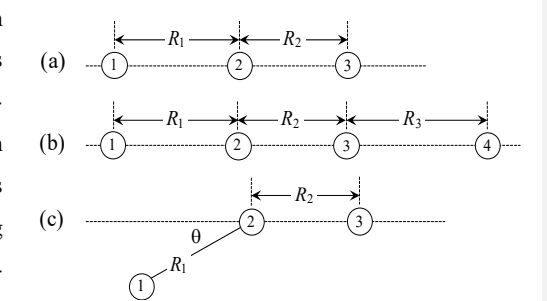


Figure 2. (a) 3 atoms in a linear configuration. (b) 4 atoms in a linear configuration. (c) 3-atom bent configurations included $\theta^0 = 30^\circ$, 60° , and 90° , and a T-shaped starting geometry. Initial interatomic distances satisfy $R_2^0 \le R_1^0$ and $R_2^0 \le R_3^0$.

using the surface-hopping approach. In our simulations, the nulcei follow the lowest triplet adiabat and the electrons instantaneously adjust to the nuclear positions. This overestimates the rate of exciton hopping between sites, especially in the 10-atom cases, where there is a dense manifold of closely lying electronic states. Non-adiabatic effects will be included in our future work.

Figure 3 shows slices of the linear 3-atom lowest adiabat and a few dominant NTOs. There is initial repulsion between atoms 1 and 2 for R_1^0 values in the range 3-4 Å. Thus, atom 1 moves away, and the force on atom 2 results in translational motion of the R_2 diatom and increased vibrational kinetic energy. The latter promotes motion toward the He₂* potential minimum. It also can endow the He₂* moiety with enough energy to result in its dissociation upon its return to the barrier peak region. The initial push toward the He₂* minimum and the return to the outer turning point region is a robust and important result of the linear 3-atom simulations. The bulk of the trajectory results, including videos, are given in the SI.

The NTOs at $R_1 = 5$ Å indicate that the Rydberg electron prefers atom 1 over the R_2 diatom, whose distances in the figure are 2.7-3.0 Å. This makes sense, as these R_2 values lie high on the He₂* entrance barrier (Figure 1). The situation is more interesting for $R_1 = 2.5$ Å. The adiabat has the Rydberg electron on atom 3 for $R_2 = 2.8$, 2.9, and 3.0 Å rather than pay the energy price of the entrance barrier at 2.5 Å, i.e., were the Rydberg electron on the R_1 diatom. The case of $R_1 = 2.5$ Å and $R_2 = 2.7$ Å is a compromise. The system has least repulsion with the electron mainly on atom 1.

Figure 4a shows the most important part of the lowest adiabat insofar as creating He2*, i.e., the entrance barrier region viewed from large R_1 with $R_2 < 2$ Å. Panel (b) shows a top view of the peak region. The blue sheet dropping sharply toward small R_1 and R_2 is headed toward the region of strong binding. The grid (spacing of 0.1 Å) puts initial arrangements (R_1^0, R_2^0) in perspective insofar as where they lie on the adiabat. The linear cases we examined lie on or within the black rectangle. The gradients of the surface explain the short time dynamics. For example, the forces within the rectangle are directed mainly along R_1 . The resulting lengthening of R_1 causes R_2 to shorten. Figure 5 is the radial distribution function g(r) for liquid He. 41-43 It dictated the R_1 and R_2

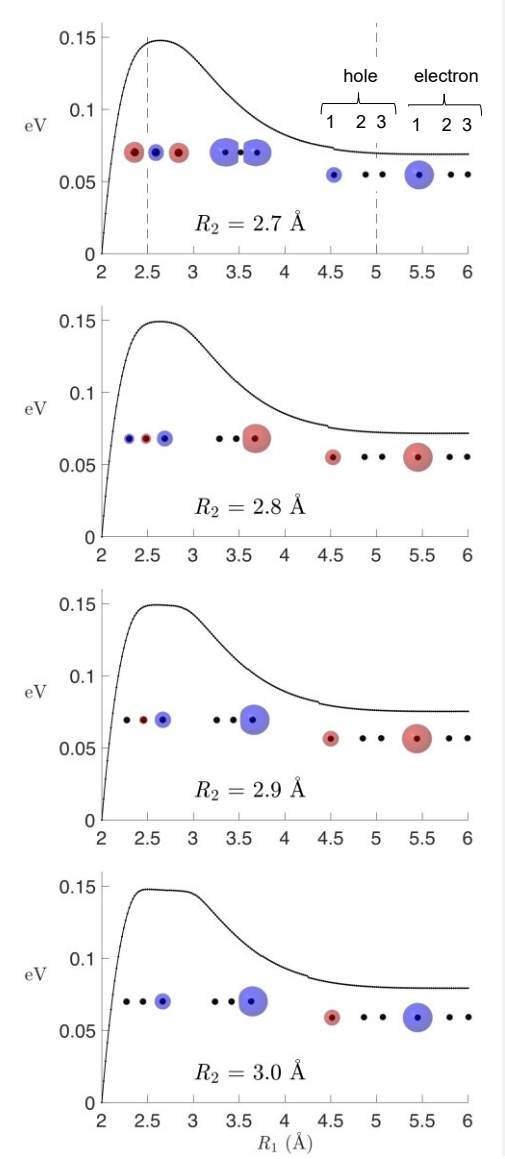


Figure 3. 1D, 3-atom lowest adiabat slices: NTOs are shown for 2.5 and 5.0 Å (note dashed lines in top panel). The NTOs show holes and electrons on the left and right as indicated in the top panel; atom labels (1,2,3) are as per Figure 2a. As with MOs, red and blue orbital colors only have meaning within an NTO (phases of \pm 1). Orbital cutoff is chosen for viewing convenience.

values used throughout.//seems repetition of the text in bottom of p.4//

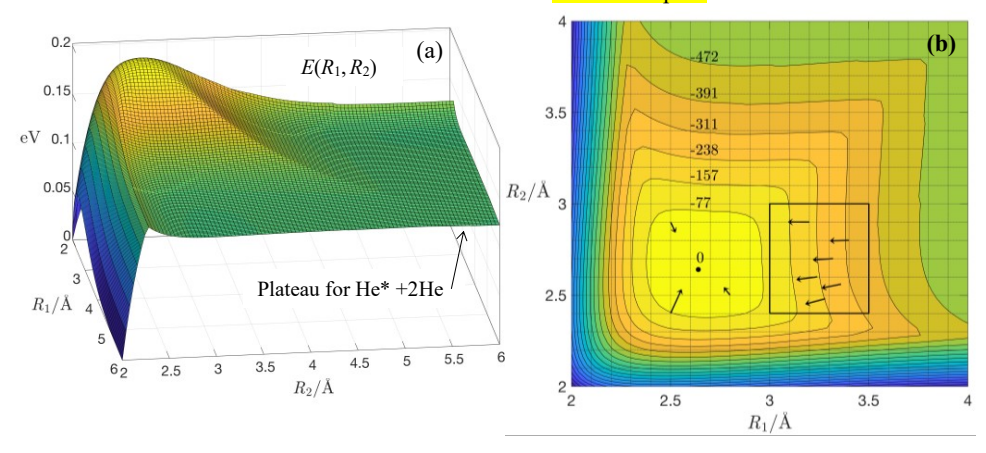


Figure 4. (a) is a view of energy versus R_1 and R_2 for 3 atoms. (b) shows a top view. The rectangle contains the (R_1^0, R_2^0) combinations used in the trajectories. Gradients enable one to see how trajectories are launched from different (R_1^0, R_2^0) . The arrows originate at the points where the gradients are evaluated.

To gain insight into exciton localization leading to He₂* formation, we propagated trajectories on the lowest triplet adiabat for many combinations of R_1^0 and R_2^0 . Figure 6a shows several representative cases. Note the $R_2(t)$ oscillation as He₂* and He move away from one another (R₁(t)). The long oscillation periods relative to the $\approx 20 \ fs$ period for energies near the bottom of the $a^3\Sigma_u^+$ well reflect the highly anharmonic oscillation due to He₂* being created high in the $a^3\Sigma_u^+$ potential. Values of R_2^0 smaller than 2.6 Å always yield He₂*.

For $(R_1^0, R_2^0) = (3.2, 2.7)$ in Figure 6a, the system encounters a deep well before returning to the bar-

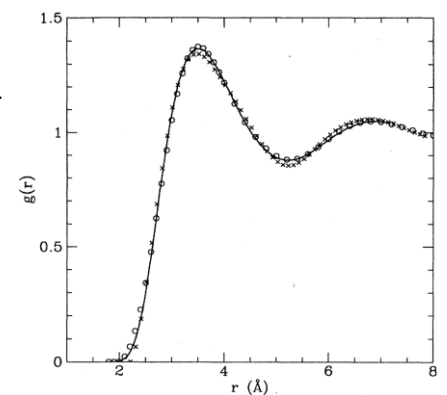


Figure 5. The smooth curve is the calculated radial distribution function g(r) for helium at 1.21 K.⁴¹ Points show experimental data.^{42,43} With permission of author, D. Ceperley.

rier peak region. The He₂* moiety gained internal energy due to R_1 repulsion early in the trajectory. Thus, dissociation takes place when $R_2(t)$ returns to the region of the barrier peak. The same

is true for $R_1^0 = 3.3 - 3.5$ Å with R_2^0 at 2.7 Å, and for $R_1^0 = 3.0 - 3.5$ Å with $R_2^0 = 2.8$ Å. The traces in these dissociative cases are indistinguishable from the one for $(R_1^0, R_2^0) = (3.2, 2.7)$.

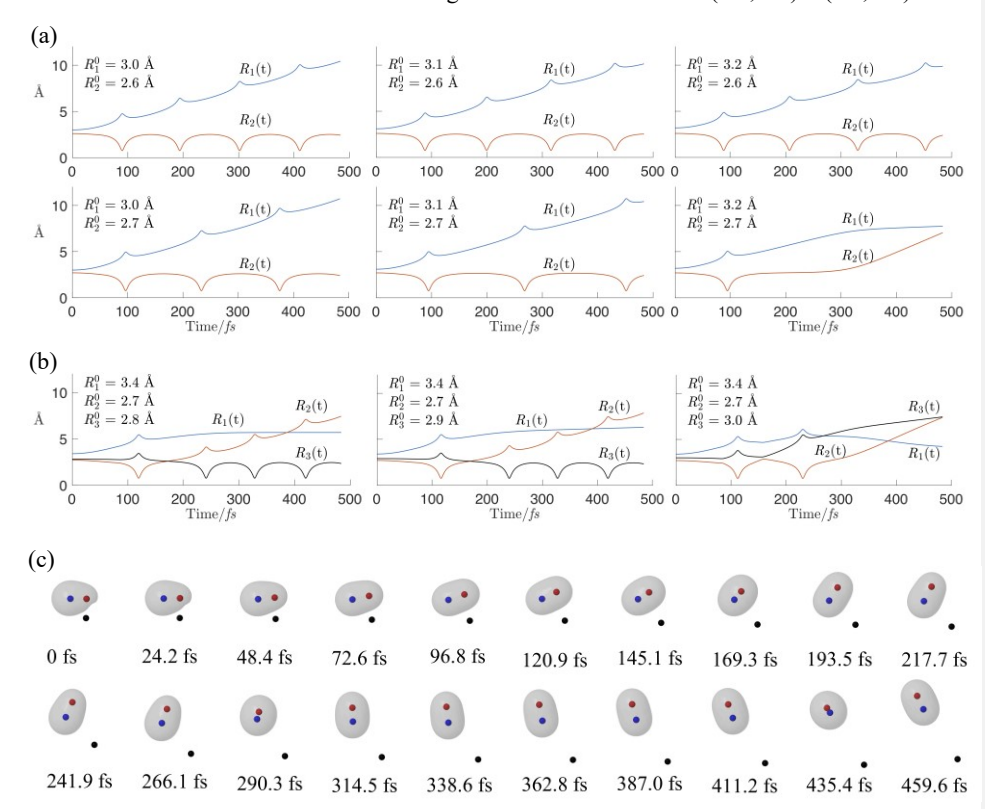


Figure 6. Trajectories for (a) linear 3-atom cases (Figure 2a), and (b) linear 4-atom cases (Figure 2b). Note that $R_2(t)$ oscillation transfers to $R_3(t)$ in the first two panels. (c) Snapshots of a trajectory for 3-atoms with $R_1^0 = 3.1$ Å, $R_2^0 = 2.5$ Å, and $\theta^0 = 90^\circ$ (Figure 2c). Smaller initial distances (R_2^0) are characteristic of the rising part of g(r). Larger initial distances (R_1^0) are characteristic of the peak region of g(r).

The above examples capture the gist of He_2^* creation for the chosen 3-atom (R_1^0, R_2^0) combinations. The R_2 pair always entered the region of strong binding, as evidenced by its rapid inward and outward passages through the region of the potential minimum. There were no exceptions. The R_2 pair did not always remain intact, however. Such results invite ponder. Might a fourth atom stabilize He_2^* by removing some of its internal energy? After all, with 3 atoms there was

limited opportunity to remove enough energy from He₂* to prevent dissociation upon its return to the barrier region.

The 4-atom configurations were examined for symmetric ($R_1^0 = R_3^0$) and non-symmetric ($R_1^0 \neq R_3^0$) arrangements (Figure 2b). For the symmetric arrangements (not shown), the middle two atoms pass through the region of the potential minimum. For $R_2^0 = 2.7$ Å, all R_1^0 values yielded He₂*; for $R_2^0 = 2.8$ Å, $R_1^0 = 3.1$ –3.3 Å yielded He₂*; and for $R_2^0 = 2.9$ Å, $R_1^0 = 3.1$ and 3.2 Å yielded He₂*. Non-symmetric arrangements are interesting (Figure 6b). Exciton transfer took place in 10 of the 24 initial configurations. The bottom line is that He₂* is easily stabilized.

Trajectories for nonlinear 3-atom cases used $\theta^0 = 30^\circ$, 60° , 90° (Figure 2c), and T-shaped initial configurations. The results for 30° were close to those for the corresponding 1D 3-atom cases. For 90° , even when the diatom initially localizes the exciton, it is discouraged from bonding because of the angular momentum it receives by being pushed from outside its center-of-mass. For $R_2^0 = 2.5$ Å, $\theta^0 = 90^\circ$, and R_1^0 values of 3.0 - 3.5 Å, He_2^* survived in all cases except $R_1^0 = 3.2$ Å. Figure 6c shows snapshots of the trajectory for $R_2^0 = 2.5$ Å, $\theta^0 = 90^\circ$, and $R_1^0 = 3.1$ Å. For $R_2^0 = 2.6$ Å and $\theta^0 = 90^\circ$, only $R_1^0 = 3.5$ Å yielded He_2^* , and for $R_2^0 = 2.7 - 2.9$ Å and $\theta^0 = 90^\circ$, He_2^* did not survive in any of the trajectories. For T-shaped starting geometries, exciton localization at the diatom was retained and the third atom and He_2^* simply moved apart.

Nine 10-atom trajectories on the lowest energy adiabat were calculated. In each case, highly vibrationally excited He₂* was formed in < 100 fs (see SI). This system features a dense manifold of excited states with multiple crossings and seams. On occasion, a pair of ground state He atoms happens to have a separation slightly smaller than the He₂* outer turning point. This arises amidst the turmoil created by electronic excitation. The exciton then moves to the new pair: He₂* + He'-He' \rightarrow He-He + He'₂*. //I guess primes should be introduced. No primes in the following text used.// In other words, the exciton hops when a He-He pair with smaller internuclear separation appears on the scene, whereas hopping probability decays exponentially with distance between sites. ⁴⁴ This artifact will be eliminated in future work by including non-adiabatic transitions. Note that He₂* yield is not affected by exciton hopping. Namely, He₂* is forthcoming regardless of whether the original He₂* transfers its exciton to a He-He pair.

The computational results are summarized as follows. In the linear and $\theta^0 = 30^\circ$ 3-atom cases, propagation on the lowest triplet adiabat using R_1^0 and R_2^0 values in accord with g(r) results in a

diatom being pushed toward the He₂* potential minimum. Stabilization of the He₂* moiety formed with the assistance of the push is achieved with an atom on the opposite side. Sideways arrangements ($\theta^0 = 90^\circ$ and T-shaped) are repulsive. Preliminary results with 10-atom cases indicate facile He₂* production.

Statistics is central to the conversion of He* to He₂*. Suppose the probability of creating He₂* is equal to the probability that excitation takes place at a He atom that has at least one nearest neighbor closer than 2.9 Å. We estimate, using g(r), that roughly 16% of the nearest neighbors along a radial direction meet this requirement. For 9 nearest neighbors, ⁴⁵ this yields a probability of $1 - (1 - 0.16)^9 = 0.8$. The real probability tends larger because of the initial compression brought about by repulsive forces. It tends smaller if 2.9 Å is reduced.

We conclude that the creation of He* in large helium droplets is followed by rapid, efficient production of highly vibrationally excited He₂*, despite a large barrier in the corresponding gas phase association reaction (Figure 1). The He₂* forms a bubble that travels to the droplet surface where it participates in the creation of He₄⁺. Future goals include larger systems, inclusion of non-adiabatic transitions, and more sophisticated sampling of initial conditions.

Computational Details

Calculations were carried out using the Q-Chem electronic structure package. $^{46\text{-}47}$ The $a^3\Sigma_u^+$ and $c^3\Sigma_g^+$ curves and the adiabats were computed using the equation-of-motion for excitation energies coupled-cluster approach with single and double excitations (EOM-EE-CCSD). $^{35\text{-}36}$ We used the doubly augmented Dunning double- ζ basis set (d-aug-cc-pVDZ). Vibrational probability densities for $a^3\Sigma_u^+$ were computed using the 'eig' function in MATLAB (see SI for details).

Commented [MOU1]: Double augmentation came later, Dunning only came up with aug-cc-PVDZ, someone else later added more functions to it. So, Dunning is placed here correctly I think.

ASSOCIATED CONTENT

Supporting Information

The Supporting Information is available free of charge on the ACS Publications website at DOI: 10.1021/acs.jpclett.8b01062

AUTHOR INFORMATION

Corresponding Authors

- * Curt Wittig, wittig@usc.edu, (213) 740-7368
- * Andrey Vilesov, vilesov@usc.edu, (213) 821-2936

Notes

The authors declare no competing financial interest.

ACKNOWLEDGMENTS

This work was supported by National Science Foundation grants CHE-1362535 (AFV), CHE-1664990 (AFV), CHE-1565704 (NP and OVP), CHE-0652830 (CW), Army Research Office grant W911NF-16-1-0232 (AIK), a 2019 Simons Fellowship in Theoretical Physics (AIK), and a Bessel Award from the Alexander von Humboldt Foundation (AIK).

REFERENCES

- (1) Toennies, J. P.; Vilesov, A. F. Superfluid Helium Droplets: A Uniquely Cold Nanomatrix for Molecules and Molecular Complexes. *Angew. Chem. Int. Ed.* **2004**, *43*, 2622-2648.
- (2) Choi, M. Y.; Douberly, G. E.; Falconer, T. M.; Lewis, W. K.; Lindsay, C. M.; Merritt, J. M.; Stiles, P. L.; Miller, R. E. Infrared Spectroscopy of Helium Nanodroplets: Novel Methods for Physics and Chemistry. *Int. Rev. Phys. Chem.* **2006**, *25*, 15-75.
- (3) Callegari, C.; Ernst, W. E., Helium Droplets as Nanocryostats for Molecular Spectroscopy From the Vacuum Ultravoilet to the Microwave Regime. In *Handbook of High-Resolution Spectroscopy*, F. Merkt, M. Q., Ed. John Wiley & Sons: Chichester, 2011; Vol. 3, pp 1551-1594.
- (4) Stienkemeier, F.; Lehmann, K. K. Spectroscopy and Dynamics in Helium Nanodroplets. *J. Phys. B* **2006**, 39, R127-R166.
- (5) Tiggesbaumker, J.; Stienkemeier, F. Formation and Properties of Metal Clusters Isolated in Helium Droplets. *Phys. Chem. Chem. Phys.* **2007**, *9*, 4748-4770.
- (6) Tanyag, R. M.; Jones, C. F.; Bernando, C.; O'Connell, S. M. O.; Verma, D.; Vilesov, A. F., Experiments with Large Superfluid Helium Nanodroplets. In *Cold Chemistry: Molecular Scattering and Reactivity Near Absolute Zero*, Osterwalder, A.; Dulieu, O., Eds. Royal Society of Chemistry: Cambridge, 2017; pp 389-443.
- (7) Gspann, J. Electron-Impact on Helium Clusters Metastable Excitation, Ionization, and Charged Mini-Cluster Ejection. *Surface Science* **1981**, *106*, 219-224.
- (8) Buchenau, H.; Knuth, E. L.; Northby, J.; Toennies, J. P.; Winkler, C. Mass-Spectra and Time-of-Flight Distributions of Helium Cluster Beams. *J. Chem. Phys.* **1990**, *92*, 6875-6889.
- (9) Buchenau, H.; Toennies, J. P.; Northby, J. A. Excitation and Ionization of ⁴He Clusters by Electrons. *J. Chem. Phys.* **1991**, *95*, 8134-8148.
- (10) Callicoatt, B. E.; Forde, K.; Jung, L. F.; Ruchti, T.; Janda, K. C. Fragmentation of Ionized Liquid Helium Droplets: A New Interpretation. *J. Chem. Phys.* **1998**, *109*, 10195-10200.
- (11) Gomez, L. F.; Loginov, E.; Sliter, R.; Vilesov, A. F. Sizes of Large He Droplets. J. Chem. Phys. 2011, 135.
- (12) Renzler, M.; Daxner, M.; Weinberger, N.; Denifl, S.; Scheier, P.; Echt, O. On Subthreshold Ionization of Helium Droplets, Ejection of He⁺, and the Role of Anions. *Phys. Chem. Chem. Phys.* **2014**, *16*, 22466-22470.
- (13) Schobel, H.; Bartl, P.; Leidlmair, C.; Denifl, S.; Echt, O.; Mark, T. D.; Scheier, P. High-Resolution Mass Spectrometric Study of Pure Helium Droplets, and Droplets Doped with Krypton. *Euro. Phys. J. D* **2011**, *63*, 209-214.
- (14) Seong, J.; Janda, K. C.; Halberstadt, N.; Spiegelmann, F. Short-Time Charge Motion in He_n⁺ Clusters. *J. Chem. Phys.* **1998**, *109*, 10873-10884.
- (15) Von Issendorff, B.; Haberland, H.; Frochtenicht, R.; Toennies, J. P. Spectroscopic Observation of a Metastable Electronically Excited He₄⁺. *Chem. Phys. Lett.* **1995**, *233*, 23-27.
- (16) Keto, J. W.; Soley, F. J.; Stockton, M.; Fitzsimm.Wa. Dynamic Properties of Neutral Excitations Produced in Electron-Bombarded Superfluid-Helium .1. He(2³S) and He₂(A ³Σ) Atomic and Molecular Metastable States. *Phys. Rev. A* **1974**. *10*. 872-886.
- (17) Keto, J. W.; Soley, F. J.; Stockton, M.; Fitzsimmons, W. A. Dynamic Properties of Neutral Excitations Produced in Electron-Bombarded Superfluid-Helium .2. Afterglow Fluorescence of Excited Helium Molecules. *Phys. Rev. A* **1974**, *10*, 887-896.
- (18) Keto, J. W.; Stockton, M.; Fitzsimmons, W. A. Dynamics of Atomic and Molecular Metastable States Produced in Electron-Bombarded Superfluid-Helium. *Phys. Rev. Lett.* **1972**, *28*, 792-795.
- (19) Hill, J. C.; Heybey, O.; Walters, G. K. Evidence of Metastable Atomic and Molecular Bubble States in Electron-Bombarded Superfluid Liquid Helium. *Phys. Rev. Lett.* **1971**, *26*, 1213-1216.
- (20) Brooks, R. L.; Hunt, J. L.; Tokaryk, D. W. Absorption-Spectra from High Vibrational Levels of He₂. *J. Chem. Phys.* **1989**, *91*, 7408-7414.
- (21) Hu, C. C. Photodetachment of Metastable Helium Molecules from Helium Clusters. Universoty of Rhode Island, 1999.
- (22) Jiang, T.; Kim, C.; Northby, J. A. Studies of Metastably Excited Helium Clusters. Surf. Rev. and Lett. 1996, 3, 377-381.
- (23) Kim, C. Photodetachment Studies of Negatively Charged and Metastably Excited Helium Nanodroplets. University of Rhode Island, 1997.
- (24) Yurgenson, S.; Hu, C. C.; Kim, C.; Northby, J. A. Detachment of Metastable Helium Molecules from Helium Nanodroplets. *Euro. Phys. J. D* **1999**, *9*, 153-157.

- (25) Knowles, P. J.; Murrell, J. N. The Metastable Quartet State of He₄⁺. J. Chem. Phys. 1995, 102, 9442-9443.
- (26) Knowles, P. J.; Murrell, J. N. The Structures and Stabilities of Helium Cluster Ions. *Mol. Phys.* **1996**, *87*, 827-833.
- (27) Fine, J.; Verma, D.; Jones, C. F.; Wittig, C.; Vilesov, A. F. Formation of He₄⁺ via Electron Impact of Helium Droplets. *J. Chem. Phys.* **2018**, *148*, 044302-1-14.
- (28) Fiedler, S. L.; Eloranta, J. Interaction of Helium Rydberg State Atoms with Superfluid Helium. *J. Low Temp. Phys.* **2014**, *174*, 269-283.
- (29) Eloranta, J.; Apkarian, V. A. The Triplet He₂* Rydberg States and Their Interaction Potentials with Ground State He Atoms. *J. Chem. Phys.* **2001**, *115*, 752-760.
- (30) Eloranta, J.; Schwentner, N.; Apkarian, V. A. Structure and Energetics of He₂* Bubble-States in Superfluid ⁴He. *J. Chem. Phys.* **2002**, *116*, 4039-4053.
- (31) Focsa, C.; Bernath, P. F.; Colin, R. The low-lying states of He₂. *Journal of Molecular Spectroscopy* **1998**, 191, 209-214.
- (32) Pavanello, M.; Cafiero, M.; Bubin, S.; Adamowicz, L. Accurate Born-Oppenheimer calculations of the low-lying $c^3\Sigma_g^+$ and a $^3\Sigma_u^+$ excited states of helium dimer. *International Journal of Quantum Chemistry* **2008**, *108*, 2291-2298.
- (33) Yarkony, D. R. On the Quenching of Helium 2 3 S Potential-Energy Curves for, and Nonadiabatic, Relativistic, and Radiative Couplings between, the A $3\Sigma_{U}^+$, A $1\Sigma_{U}^+$, B $^3\Pi_g$, B $^1\Pi_g$, C $^3\Sigma_g^+$, and C $^1\Sigma_g^+$ States of He₂. *J. Chem. Phys.* **1989**, *90*, 7164-7175.
- (34) Hartmann, M.; Miller, R. E.; Toennies, J. P.; Vilesov, A. Rotationally Resolved Spectroscopy of SF₆ in Liquid-Helium Clusters a Molecular Probe of Cluster Temperature. *Phys. Rev. Lett.* **1995**, *75*, 1566-1569.
- (35) Bartlett, R. J. Coupled-cluster theory and its equation-of-motion extensions. *Wiley Interdisciplinary Reviews-Computational Molecular Science* **2012**, *2*, 126-138.
- (36) Krylov, A. I. Equation-of-Motion Coupled-Cluster Methods for Open-Shell and Electronically Excited Species: The Hitchhiker's Guide to Fock Space. *Ann. Rev. Phys. Chem.* **2008**, *59*, 433-462.
- (37) Luzanov, A. V.; Sukhorukov, A. A.; Umanskii, V. E. Application of Transition Density Matrix for Analysis of the Excited States. *Theor. Exp. Chem.* **1976**, *10*, 354-361.
- (38) Mewes, S. A.; Plasser, F.; Krylov, A.; Dreuw, A. Benchmarking Excited-State Calculations Using Exciton Properties. *J. Chem. Theor. Comput.* **2018**, *14*, 710-725.
- (39) Plasser, F.; Wormit, M.; Dreuw, A. New Tools for the Systematic Analysis and Visualization of Electronic Excitations. I. Formalism. *J. Chem. Phys.* **2014**, *141*, 024106.
- (40) Martin, R. L. Natural Transition Orbitals. *J. Chem. Phys.* **2003**, *118*, 4775-4777.
- (41) Ceperley, D. M. Path-Integrals in the Theory of Condensed Helium. Rev. Mod. Phys. 1995, 67, 279-355.
- (42) Svensson, E. C.; Sears, V. F.; Woods, A. D. B.; Martel, P. Neutron-Diffraction Study of the Static Structure Factor and Pair Correlations in Liquid ⁴He. *Phys. Revi. B* **1980**, *21*, 3638-3651.
- (43) Robkoff, H. N.; Hallock, R. B. Structure-Factor Measurements in ⁴He at Saturated Vapor-Pressure for 1.38 < T < 4.24 K. *Phys. Rev. B* **1981**, *24*, 159-182.
- (44) Agranovich, V. M., *Excitations in Organic Solids*. International Series of Monographs on Physics. Oxford University Press: Oxford, UK, 2009; Vol. 142.
- (45) Henshaw, D. G. Effect of the Lambda-Transition on the Atomic Distribution in Liquid Helium by Neutron Diffraction. *Phys. Rev.* **1960**, *119*, 9-13.
- (46) Shao, Y. H.; Gan, Z. T.; Epifanovsky, E.; Gilbert, A. T. B.; Wormit, M.; Kussmann, J.; Lange, A. W.; Behn, A.; Deng, J.; Feng, X. T.; Ghosh, D.; Goldey, M.; Horn, P. R.; Jacobson, L. D.; Kaliman, I.; Khaliullin, R. Z.; Kus, T.; Landau, A.; Liu, J.; Proynov, E. I.; Rhee, Y. M.; Richard, R. M.; Rohrdanz, M. A.; Steele, R. P.; Sundstrom, E. J.; Woodcock, H. L.; Zimmerman, P. M.; Zuev, D.; Albrecht, B.; Alguire, E.; Austin, B.; Beran, G. J. O.; Bernard, Y. A.; Berquist, E.; Brandhorst, K.; Bravaya, K. B.; Brown, S. T.; Casanova, D.; Chang, C. M.; Chen, Y. Q.; Chien, S. H.; Closser, K. D.; Crittenden, D. L.; Diedenhofen, M.; DiStasio, R. A.; Do, H.; Dutoi, A. D.; Edgar, R. G.; Fatehi, S.; Fusti-Molnar, L.; Ghysels, A.; Golubeva-Zadorozhnaya, A.; Gomes, J.; Hanson-Heine, M. W. D.; Harbach, P. H. P.; Hauser, A. W.; Hohenstein, E. G.; Holden, Z. C.; Jagau, T. C.; Ji, H. J.; Kaduk, B.; Khistyaev, K.; Kim, J.; Kim, J.; King, R. A.; Klunzinger, P.; Kosenkov, D.; Kowalczyk, T.; Krauter, C. M.; Lao, K. U.; Laurent, A. D.; Lawler, K. V.; Levchenko, S. V.; Lin, C. Y.; Liu, F.; Livshits, E.; Lochan, R. C.; Luenser, A.; Manohar, P.; Manzer, S. F.; Mao, S. P.; Mardirossian, N.; Marenich, A. V.; Maurer, S. A.; Mayhall, N. J.; Neuscamman, E.; Oana, C. M.; Olivares-Amaya, R.; O'Neill, D. P.; Parkhill, J. A.; Perrine, T. M.; Peverati, R.; Prociuk, A.; Rehn, D. R.; Rosta, E.; Russ, N. J.; Sharada, S. M.; Sharma, S.; Small, D. W.; Sodt, A.; Stein, T.; Stuck, D.; Su, Y. C.; Thom, A. J. W.; Tsuchimochi, T.; Vanovschi, V.; Vogt, L.; Vydrov, O.; Wang, T.; Watson, M. A.; Wenzel, J.; White, A.; Williams, C. F.; Yang, J.; Yeganeh, S.; Yost, S. R.; You, Z. Q.; Zhang, I. Y.; Zhang, X.;

Zhao, Y.; Brooks, B. R.; Chan, G. K. L.; Chipman, D. M.; Cramer, C. J.; Goddard, W. A.; Gordon, M. S.; Hehre, W. J.; Klamt, A.; Schaefer, H. F.; Schmidt, M. W.; Sherrill, C. D.; Truhlar, D. G.; Warshel, A.; Xu, X.; Aspuru-Guzik, A.; Baer, R.; Bell, A. T.; Besley, N. A.; Chai, J. D.; Dreuw, A.; Dunietz, B. D.; Furlani, T. R.; Gwaltney, S. R.; Hsu, C. P.; Jung, Y. S.; Kong, J.; Lambrecht, D. S.; Liang, W. Z.; Ochsenfeld, C.; Rassolov, V. A.; Slipchenko, L. V.; Subotnik, J. E.; Van Voorhis, T.; Herbert, J. M.; Krylov, A. I.; Gill, P. M. W.; Head-Gordon, M. Advances in molecular quantum chemistry contained in the Q-Chem 4 program package. *Mol. Phys.* 2015, *113*, 184-215. (47) Krylov, A. I.; Gill, P. M. W. Q-Chem: an Engine for Innovation. *Wiley Interdisciplinary Reviews-Comput. Mol. Sci.* 2013, *3*, 317-326.